REFERENCES AND NOTES

1. For recent reviews, see: W. H. Miller, *Annu. Rev. Phys. Chem.* **41**, 245 (1990); *Chem. Eng. News* **68** (no. 23), 32 (1990).
2. D. A. V. Kliner, D. E. Adelman, R. N. Zare, *J. Chem. Phys.* **95**, 1648 (1991).
3. N. C. Blais, M. Zhao, D. G. Truhlar, D. W. Schwenke, D. J. Kouri, *Chem. Phys. Lett.* **166**, 11 (1990).
4. S. A. Buntin, C. F. Giese, W. R. Gentry, *ibid.* **168**, 513 (1990); R. E. Continetti, B. A. Balko, Y. T. Lee, *J. Chem. Phys.* **93**, 5719 (1990).
5. J. Z. H. Zhang and W. H. Miller, *J. Chem. Phys.* **91**, 1528 (1989); M. Zhao, D. G. Truhlar, D. W. Schwenke, D. J. Kouri, *J. Phys. Chem.* **94**, 7074 (1990).
6. D. G. Truhlar and C. J. Horowitz, *J. Chem. Phys.* **68**, 2466 (1978).
7. B. Liu, *ibid.* **58**, 1925 (1973).
8. P. Siegbahn and B. Liu, *ibid.* **68**, 1074 (1978).
9. A. J. C. Varandas, F. B. Brown, C. A. Mead, D. G. Truhlar, N. C. Blais, *ibid* **86**, 6258 (1987).
10. D. M. Ceperley and B. J. Alder, *ibid.* **81**, 5833 (1984).
11. A. I. Boothroyd, W. J. Keogh, P. G Martin, M. R. Peterson, *ibid.* **95**, 4343 (1991).
12. B. Liu, *ibid.* **80**, 581 (1984).
13. J. B. Anderson, C. A. Traynor, B. M. Boghosian, *ibid.* **95**, 7418 (1991).
14. J. B. Anderson, *ibid.* **63**, 1499 (1975).
15. D. M. Arnow, M. H. Kalos, M. A. Lee, K. E. Schmidt, *ibid.* **77**, 5562 (1982).
16. R. C. Grimm and R. G. Storer, *J. Comput. Phys* **7**, 134 (1971).
17. M. H. Kalos, *Phys. Rev. A* **128**, 1791 (1962).
18. R. N. Barnett, P J. Reynolds, W A. Lester, *J. Chem. Phys* **84**, 4992 (1986); C. J. Umrigar, K. G. Wilson, J. W. Wilkins, *Phys. Rev. Lett.* **60**, 1719 (1988), K. E. Schmidt and J. W. Moskowitz, *J Chem. Phys.* **93**, 4172 (1990).
19. W. Kolos, K. Szalewicz, H. Monkhorst, *J. Chem. Phys.* **84**, 3278 (1986).
20. E. Clementi *et al.*, *Chem. Rev.* **91**, 679 (1991).
21. This work was supported by grants from the National Science Foundation (CHE-8714613) and the Office of Naval Research (N00014-92-J-1340).

18 March 1992; accepted 10 August 1992

Infrared Reflection-Absorption Spectroscopy and STM Studies of Model Silica-Supported Copper Catalysts

Xueping Xu, Scott M. Vesecky, D. Wayne Goodman

The structure of model silica-supported copper catalysts has been investigated with scanning tunneling microscopy (STM) and infrared reflection-absorption spectroscopy (IRAS). The IRAS studies of CO on the model silica-supported copper catalysts indicate that there are several types of copper clusters with surface structures similar to (111), (110), and other high-index planes of single-crystal copper. The STM studies show several types of copper clusters on silica and reveal images of metal clusters on an amorphous oxide support with atomic resolution.

The activity and selectivity of many metal-catalyzed reactions often are sensitive to the metal particle morphology (*1*). However, there are no direct techniques to determine the surface structure of supported metal catalysts with atomic resolution. Scanning and transmission electron microscopies (SEM and TEM) are widely used to examine catalysts, but SEM does not have sufficient resolution for atomic imaging, whereas TEM requires thin samples and only yields a projected image (*2*). Infrared absorption spectroscopy (IRAS) is also often used to characterize adsorbed species in situ, and the structure of the metal surface in certain cases can be inferred when the characteristic frequencies of an adsorbate on different crystal faces are available (*3*).

Scanning tunneling and atomic force microscopies (STM and AFM) are powerful techniques that directly probe the surface with atomic resolution (*4*). Although STM has successfully imaged metal and semiconductor single-crystal surfaces and epitaxially grown metal films, atomically resolved images of metal particles supported on an amorphous oxide surface have yet to be reported. Typical catalyst support materials consist of amorphous oxides. Low-resolution STM images of an oxide-supported metal catalyst have been obtained (*5*).

We report atomically resolved STM images of a model silica-supported copper (Cu/SiO_2) catalyst that include atomic-level images for metal particles on an amorphous substrate. Complementary IRAS studies of CO on the Cu/SiO_2 are also presented (*6*–*8*).

The SiO_2 films, whose preparation on Mo(110) has been reported previously (*9*), were characterized with Auger electron, x-ray photoelectron, electron energy loss, IRAS, and thermal programmed desorption (TPD) spectroscopies (*9*, *10*). The films (~100 Å thick) are thermally stable up to 1600 K, exhibit properties of vitreous SiO_2, and have been shown to be valid models for the SiO_2 surface (*9*, *10*). The SiO_2 films grow initially in a layer-by-layer fashion for the first few layers, fully covering the Mo(110) substrate (*9*, *10*). The coverage of Cu (θ_{Cu}) in all cases reported here was determined with TPD (*7*). After evaporative deposition, the Cu films were annealed to 700 K and cooled to 300 K before being transferred to air for STM and AFM studies.

A series of IRAS spectra of CO chemisorbed on several Cu/SiO_2 catalysts is shown in Fig. 1. The Cu was deposited onto the SiO_2 thin film at 100 K, annealed to 900 K, cooled to 90 K, and then saturated with CO. At low θ_{Cu} [<0.3 monolayer (ML)], two IR bands are apparent at 2110 and 2062 cm^{-1}. As θ_{Cu} was increased from 1.1 to 3.4 ML, a new IR band appeared at 2094 cm^{-1}, and the band at 2062 cm^{-1} shifted to 2074 cm^{-1}. At 15 ML of Cu, a prominent band was observed at 2102 cm^{-1}, with two shoulders at 2087 and 2070 cm^{-1}. Upon heating to 900 K, evaporated Cu forms three-dimensional (3-D) clusters on SiO_2 with a dispersion of ~0.4 at an effective θ_{Cu} of 2 ML (*8*). These IR bands can then be assigned to specific CO adsorption sites directly related to distinct morphologies of the 3-D Cu clusters.

Adsorption of CO on Cu single-crystal surfaces has been extensively studied by IRAS. Adsorption on low-index Cu planes

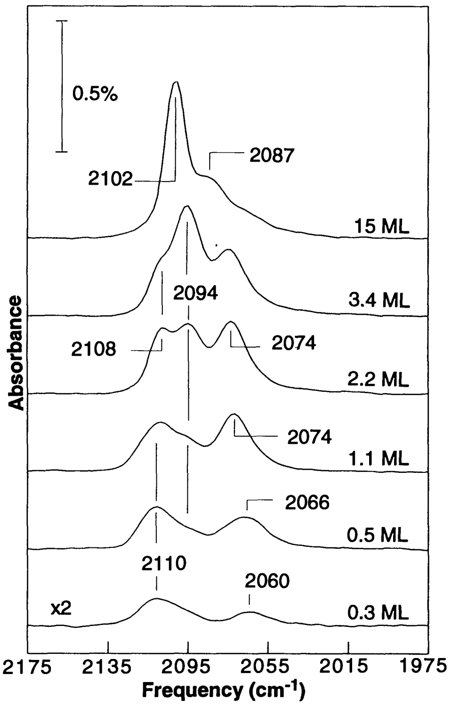

Fig. 1. Infrared reflection-absorption spectra of CO on copper/silica (100 Å)/Mo(110). Copper was deposited at 90 K and annealed to 900 K. The Cu coverages are 0.3, 0.5, 1.1, 2.2, 3.4, and 15 monolayers, respectively (ML; 1 ML = 1.3×10^{15} atom/cm^2). Carbon monoxide was adsorbed at 90 K to saturation.

Department of Chemistry, Texas A&M University, College Station, TX 77843–3255.

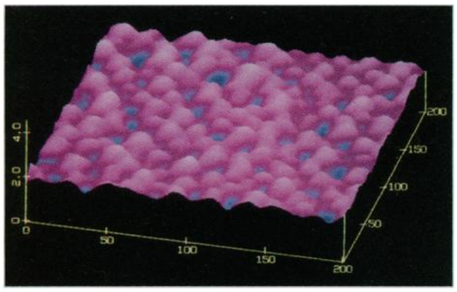

Fig. 2. A 2000 Å by 2000 Å AFM image of 15 ML of Cu on silica (100 Å)/Mo(110). The Cu cluster size is ~200 Å.

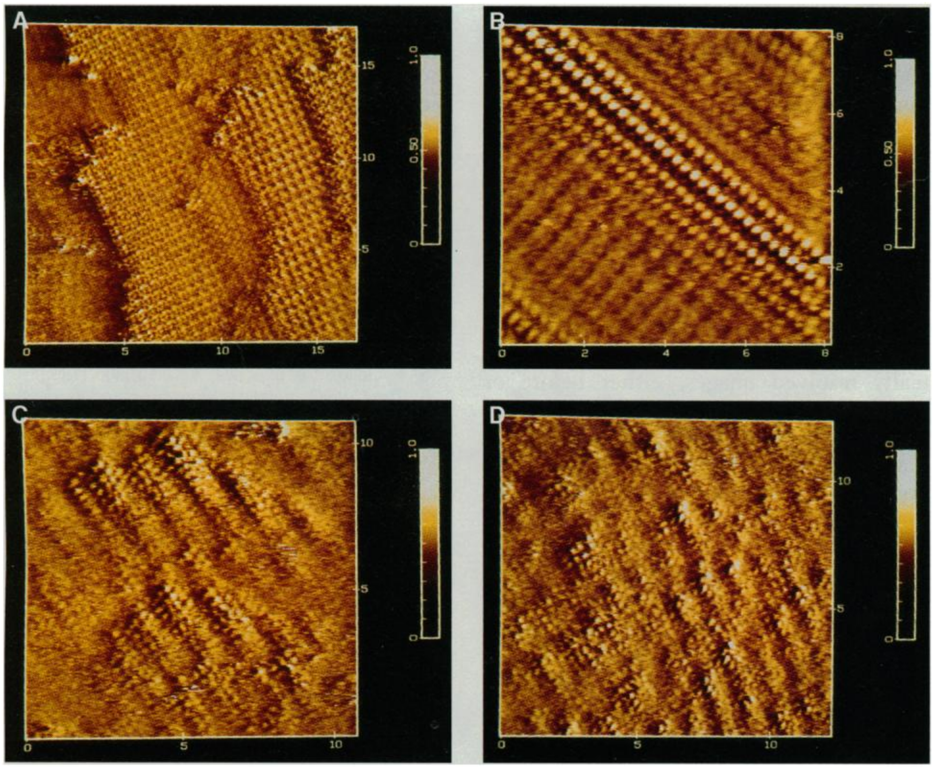

Fig. 3. STM images of four areas of 0.6 ML Cu on silica (100 Å)/Mo(110). (**A**) A 170 Å by 170 Å image of a near square lattice with Cu-Cu spacing of 6.0 Å by 5.4 Å. (**B**) A 80 Å by 80 Å image of a rectangular lattice with Cu-Cu spacing of 5.4 Å by 2.9 Å. (**C**) A 110 Å by 110 Å and a (**D**) 120 Å by 120 Å images of disordered copper clusters with interatomic spacing of 2.8 to 3.8 Å. These images were acquired after the sample was immersed in water and dried in air.

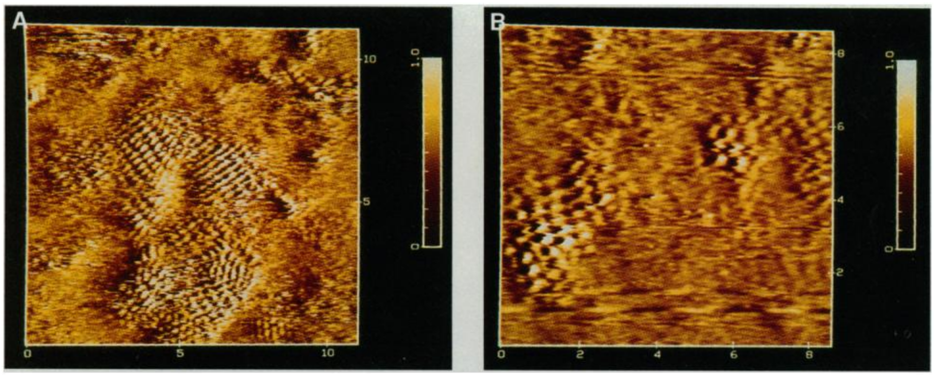

Fig. 4. STM images of 1.2 ML Cu on silica (100 Å)/Mo(110). (**A**) A 110 Å by 110 Å image of a cluster with a Cu-Cu spacing of 4.4 Å by 2.4 Å. This image was acquired after the sample was exposed to water and dried in air. (**B**) A 90 Å by 90 Å image of the freshly prepared sample, prior to immersion in water.

exhibits distinctive CO stretching frequencies (*11–18*). For example, the CO stretch frequency is 2070 cm^{-1} on Cu(111) (*12, 13*), 2093 cm^{-1} on Cu(110) (*14–16*), and 2087 cm^{-1} on Cu(100) at saturation θ_{CO} (*12, 17, 18*). Furthermore, CO adsorption on the high-index Cu(211), Cu(311), and Cu(755) planes has also been investigated (*11*). A symmetric narrow band centered at 2110 cm^{-1} is observed on Cu(211) at saturation θ_{CO}, whereas a doublet is evident at low θ_{CO} (*11*). The CO stretch frequencies are 2104 and 2106 cm^{-1} for saturation θ_{CO} on Cu(311) and Cu(755), respectively (*11*), whereas on evaporated Cu films, CO typically exhibits a band at 2102 cm^{-1} (*19*). The high-index surfaces as well as the Cu films have high densities of step sites, which typically yield a CO stretching frequency of ~2102 cm^{-1} (*3, 11, 19*) at saturation θ_{CO}.

A comparison of the IR spectra for CO adsorbed on Cu/SiO_2 (Fig. 1) with those for CO on the single-crystal surfaces suggests that the Cu/SiO_2 catalysts have distinctive crystalline facets. Specifically, the lowest frequency band (~2074 cm^{-1}) is attributed to a (111)-like structure, the 2094 cm^{-1} band to a (110)-like structure, and the 2108 to 2110 cm^{-1} band to structures related to the high-index planes, such as (211) and (311). A band at 2087 cm^{-1}, which is only observed at high θ_{Cu}, is assigned to CO adsorption onto a Cu(100)-like structure (*8*).

The well-resolved IR bands indicate that there are several structures for Cu/SiO_2, and these structures are associated with small clusters at low θ_{Cu}. When two different types of CO dipoles with slightly different vibrational frequencies are adjacent, the intensity of the low-frequency band is transferred to the high-frequency band through dipole coupling (*3*). For example, for a Cu(16,15,0) surface with ~6% of the surface atoms at step sites, IR spectra show that the high-frequency band is more intense, although it constitutes only a few percent of the CO adlayer at saturation (*3, 14*). Therefore, if a small Cu cluster on SiO_2 has several different adsorption sites with similar CO stretching frequencies, intensity transfer would result in one primary CO IR absorption band with one or more low-frequency shoulders. The well-resolved bands for the low-θ_{Cu} films (<3.4 ML) strongly suggest that there are several types of small Cu clusters, with each θ_{Cu} exhibiting clusters with one dominant structure. At high θ_{Cu} (15 ML), AFM images show that the Cu grains are ~200 Å in diameter and contiguous (Fig. 2). IRAS of CO adsorbed on this film exhibits only one major band at 2102 cm^{-1}, attributed to CO adsorption onto step sites. The relatively low intensity of the other IR bands is due to intensity transfer from these features to the step sites.

The AFM image of a thin Cu film (~15 ML) on SiO_2 (Fig. 2) shows that the distribution of the grain sizes of the Cu at this coverage is very uniform with an average size of ~200 Å. The SiO_2 film also exhibits some long-range features with an average size of ~2000 Å. Within each grain, the SiO_2 surface appears to be smooth and flat, although atomic resolution of SiO_2 was not obtained.

The STM images in Fig. 3 are of a SiO_2

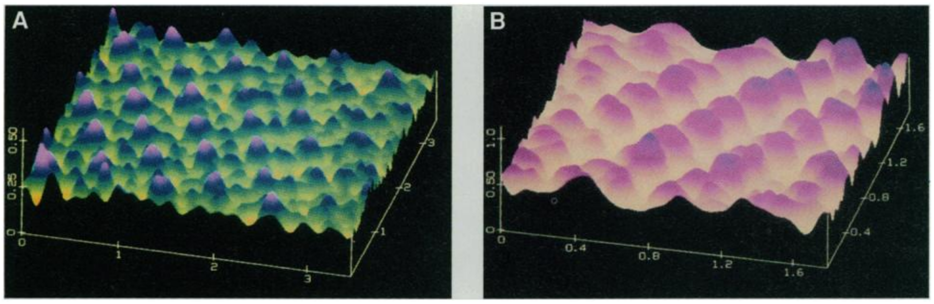

Fig. 5. (**A**) A 35 Å by 35 Å topographic image of the cluster shown in Fig. 3A. (**B**) A 17 Å by 17 Å topographic image of a cluster shown in Fig. 4A.

film with $\theta_{Cu} \approx 0.6$ ML, whereas the STM images in Fig. 4 are for ~1 ML of Cu. These atomically resolved images were acquired at various locations on the samples. These images are attributed to Cu atoms on SiO_2, in that no atomic resolution was realized for a SiO_2 without Cu.

Several types of Cu clusters occur that have distinctive structures, consistent with the corresponding IRAS studies of chemisorbed CO under ultrahigh vacuum (UHV) conditions. The image in Fig. 3A exhibits a near square lattice with a spacing of ~6.0 Å by 5.4 Å. A rectangular lattice with a spacing of ~5.4 Å by 2.9 Å is shown in Fig. 3B. Figure 3, C and D, illustrate Cu clusters without ordered structures. The distances between Cu atoms in these disordered structures are in the range of 2.8 to 3.8 Å.

High-resolution 3-D images are shown in Fig. 5 for the two Cu clusters that are displayed in Figs. 3A and 4A, respectively. The near square lattice (Figs. 3A and 5A) shows additional ordered atoms along the Cu atomic rows, although these additional atoms appear to be located in an underlying layer. A lattice spacing of 4.4 ± 0.2 Å by 2.4 ± 0.2 Å is seen in Fig. 5B, in good agreement with the lattice spacing of a Cu(311) surface, 4.42 Å by 2.55 Å (*20*).

The STM atomic images are only observed for Cu coverages on the order of 1 ML. Atomic images were not realized for a ~15-ML Cu film with STM, although AFM showed high-resolution, long-range features (Fig. 2). This difference may be due to the greater roughness of this thick Cu film compared to the thin films. For the ultrathin Cu films (~1 ML), the dispersion is very high, in the range of 0.4 to 0.5 (*8*), suggesting that Cu wets the SiO_2 surface.

Because the STM studies were performed in air, the images observed are not likely of pure Cu clusters, but rather of partially oxidized Cu. The Cu films prepared in UHV conditions have been shown to be metallic (*8*); however, upon exposure to oxygen the Cu films are partially oxidized, as shown by x-ray photoelectron spectroscopy and TPD (*10*, *20*). Therefore, upon exposure to air, the Cu films would likely be partially covered with oxygen and other impurities such as water and hydrocarbons. Exposure of the films to water improved the quality of the STM images. The STM image for a freshly prepared sample is shown in Fig. 4B, whereas Fig. 4A and Fig. 3, A to D, present the STM images for samples following immersion in water and drying in air. The clean SiO_2 films yielded no atomically resolved images, either before or after immersion in water.

Generally, the atomic spacings of Figs. 3 and 4 do not correspond to any obvious crystalline facets of metallic Cu. The spacing of 4.4 Å by 2.4 Å for the image in Fig. 4A, as noted, correlates approximately with the Cu(311) facet. Several compounds could be formed following exposure of the Cu films to air and water, for example, cupric oxide (CuO), cuprite (Cu_2O), and cupric hydroxide [$Cu(OH)_2$]. Cuprite has a cubic structure with a unit cell size of 4.27 Å (*21*). The Cu-Cu distances are 3.02 Å by 4.27 Å and 3.02 Å by 3.02 Å for the (110) and (100) facets, respectively (*21*). These distances do not match the observed atomic spacings. Cupric oxide has a monoclinic structure, with Cu-Cu distances of 2.88 Å to 3.73 Å (*21*), within the range of the atomic spacings in the images of Fig. 3, C and D. In particular, a close inspection of certain clusters in Fig. 3D reveals that some Cu atoms are arranged in a 3.0 ± 0.2 Å by 3.8 ± 0.2 Å rectangular structure, similar to the Cu rectangular spacing of 3.16 Å by 3.73 Å in the (010) plane of cupric oxide (*21*). Cupric hydroxide has an orthorhombic structure with a unit cell size of 10.59 Å by 5.26 Å by 2.95 Å (*21*). The rectangular atomic spacing of 5.4 Å by 2.9 Å in Fig. 3B is in good agreement with the Cu spacing of 5.26 Å by 2.95 Å for the (100) plane of the $Cu(OH)_2$ crystal (*21*).

The mechanism for the evolution of ordered Cu structures on an amorphous SiO_2 substrate is not well understood. The SiO_2 films do not produce ordered low-energy electron diffraction (LEED) patterns, suggesting that the films are not ordered on the scale of the coherence length of the LEED beam. However, the annealed SiO_2 films may be ordered on the scale of the small clusters, and thus could serve as a template for the growth of ordered Cu structures.

The use of SiO_2 thin films on a metal substrate as a model for a SiO_2 surface is particularly advantageous for the STM and IRAS studies. Bulk SiO_2 is an insulator, precluding its use in STM studies. Thin films of SiO_2 conduct current, probably through charge carriers, and are sufficiently smooth so that they can be successfully investigated with STM.

REFERENCES AND NOTES

1. See, for example, D. W. Goodman, *Catal. Today* **12**, 189 (1992).
2. See, for example, G. Fuchs, D. Neiman, H. Poppa, *Langmuir* **7**, 2853 (1991).
3. V. M. Browne, S. G. Fox, P. Hollins, *Catal. Today* **9**, 1 (1991).
4. P. K. Hansma and J. Tersoff, *J. Appl. Phys.* **61**, R1 (1987).
5. P. Gallezot *et al.*, *Catal. Lett.* **13**, 305 (1992).
6. The Cu/SiO_2 catalysts were prepared in an ultrahigh vacuum chamber (base pressure < 2×10^{-10} torr), equipped with a UTI quadrupole mass spectrometer, an Auger electron spectrometer, and a Mattson Cygnus 100 FTIR spectrometer (*7*). The IRAS data for CO chemisorbed onto Cu/SiO_2 were collected in the UHV chamber with a resolution of 4 cm^{-1} (*8*). The STM and AFM studies were performed with a Digital Instruments Nanoscope II with standard mechanically formed Pt-Ir STM tips and Si_3N_4 AFM cantilevers. The STM images were obtained in the constant current mode with average tip bias voltages of 22 mV and tunneling currents of 3.9 nA. Surface orientations and interatomic spacings were obtained from the unprocessed images.
7. X. Xu and D. W. Goodman, *Appl. Phys. Lett.*, in press.
8. ______, unpublished results.
9. ______, *Appl. Phys. Lett.* **61**, 774 (1992).
10. ______, unpublished results.
11. J. Pritchard, T. Catterick, R. K. Gupta, *Surf. Sci.* **76**, 1 (1975).
12. M. A. Chesters, S. F. Parker, R. Raval, *ibid.* **165**, 179 (1986).
13. B. E. Hayden, K. Kretzschmar, A. M. Bradshaw, *ibid.* **155**, 553 (1985); P. Hollins and J. Pritchard, *ibid.* **89**, 486 (1979).
14. P. Hollins, K. J. Davis, J. Pritchard, *ibid.* **138**, 75 (1984).
15. D. P. Woodruff, B. E. Hayden, K. Prince, A. M. Bradshaw, *ibid.* **123**, 397 (1982).
16. K. Horn, M. Hussain, J. Pritchard, *ibid.* **63**, 244 (1977).
17. R. Ryberg, *ibid.* **114**, 627 (1982).
18. K. Horn and J. Pritchard, *ibid.* **55**, 701 (1976).
19. P. Dumas, R. G. Tobin, P. L. Richards, *ibid.* **171**, 579 (1986).
20. J.-W. He, X. Xu, D. W. Goodman, *ibid.*, in press.
21. These distances are calculated based on the unit cell size and structure according to R. W. G. Wyckoff [*Crystal Structures* (Wiley, New York, ed. 2, 1963), vol. 1].
22. Supported by the Department of Energy, Office of Basic Energy Sciences, Division of Chemical Sciences. We thank N. Loganathan for his assistance in the acquisition of the AFM images.

29 June 1992; accepted 10 September 1992